Liquid-crystal blazed-grating beam deflector

Xu Wang, Daniel Wilson, Richard Muller, Paul Maker, and Demetri Psaltis

A transmission-type nonmechanical multiple-angle beam-steering device that uses liquid-crystal blazed grating has been developed. Sixteen steering angles with a contrast ratio of 18 has been demonstrated. A detailed analysis of the liquid-crystal and poly(methyl methacrylate) blazed-grating deflector was carried out to provide guidance during the deflector's development. A manufacturing offset compensation technique is proposed to improve the device's performance greatly. A hybrid approach utilizing electrically generated blazed grating combined with the cascading approach described here yields in excess of 500 deflecting angles. © 2000 Optical Society of America

OCIS codes: 050.1970, 230.3720, 230.2090, 050.1940.

1. Introduction

Nonmechanical beam-steering devices have many applications in optical interconnects,[1] optical fiber communication,[2] projection displays,[3] and optical data storage.[4] Recently there have been several nonmechanical beam-steering devices developed by different research groups.[5–11] With its low driving voltage and mature (low-cost) fabrication technology, liquid-crystal (LC) technology seems to be an excellent candidate for beam-steering devices. The effort in the development of LC beam deflectors can be traced back to the early 1970's. At that time, Borel *et al*.[12] patented an idea to steer the beam with a LC diffraction grating, in which the binary rectangular diffraction grating is switched on and off by the LC. Its steering efficiency is low because of the grating's binary phase. Fray and Jones[13] demonstrated another index-matching approach that used a prism as the light-coupling component. In the 1990's, Dorschner and Resler[14] patented an optical phased-array beam steerer, in which the well-known phased-array technology used in microwave radar is adopted to the optical frequency domain.[15] The similar controllable blazed-grating concept was also demonstrated by Schulze and Reden[8] and Williams *et al*.[9] Sutherland and Natarajan[16] and Domash *et al*.[10] also implemented this type of switching concept by using polymer-dispersed LC's. In this paper we propose and demonstrate a LC beam steerer that uses custom-fabricated blazed grating. Although the target application of the developed device is for a compact holographic memory system, it is also a good candidate for many other applications, such as fiber communications,[2] LC on silicon microdisplay,[17] and optical scanners.[18]

This paper is organized as follows. First the device's working mechanism and design considerations are described, and then the fabrication process is introduced. Finally, we present the characterization results and some discussion.

2. Device Description

Figure 1 is a cross-sectional view of one layer of the LC beam deflector. The device's substrate is a poly(methyl methacrylate) (PMMA) blazed grating made by direct electron-beam (e-beam) lithography[19] on top of a transparent metal indium tin oxide (ITO) coated glass. A transparent cover glass (also ITO coated) is put on top of this PMMA blazed grating, separated with fiber spacers of a few micrometers. A thin layer of nematic LC is then sandwiched in between. The ITO layer deposited underneath the PMMA grating and another ITO layer coated on the bottom surface of the cover plate are used to electrically drive the LC to change the phase information of the illuminating light. Our essential idea is to operate this LC–PMMA composite grating by exploiting the electro-optic effect of nematic LC,[20] by which its refractive index for extraordinary light can be modulated by the driving voltage. When no electric field is present, the refractive indices of the PMMA sub-

X. Wang and D. Psaltis (psaltis@caltech.edu) are with the Department of Electrical Engineering, California Institute of Technology, Pasadena, California 91125. D. Wilson, R. Muller, and P. Maker are with the Center for Space Microelectronics Technology, Jet Propulsion Laboratory, California Institute of Technology, Pasadena, California 91109-8099.

Received 5 January 2000; revised manuscript received 25 August 2000.

0003-6935/00/356545-11$15.00/0

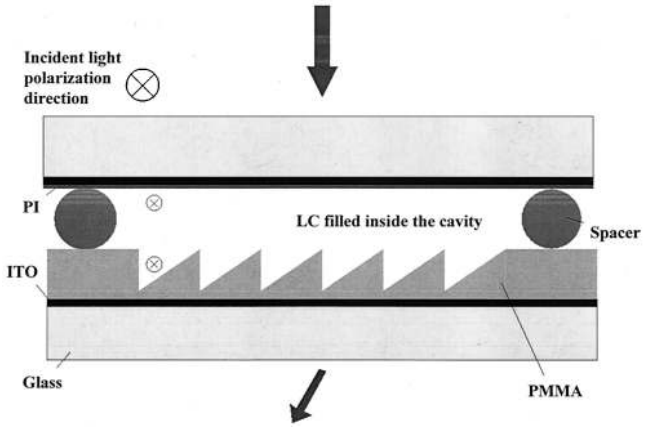

Fig. 1. LC blazed-grating beam deflector. PI, polyimide.

strate and LC are different, and strong diffraction is produced by the refractive index–phase difference of this OFF state. The diffraction efficiency is determined by the blazed-grating parameters, such as grating depth, grating period, as well as blaze profile. When an electric field is applied, the refractive index of the LC is decreased; at a certain driving voltage, index matching occurs between the PMMA and the LC. The whole LC–PMMA composite grating structure can then be considered as an optically flat plate, and no diffraction occurs for this ON state. In such a way, the device can be viewed as an electrically controlled binary switch. The incident beam can be either deflected (the OFF state) or undeflected (the ON state). Furthermore, this device belongs to the so-called polarized beam deflector because the above-described electro-optic mechanism works only for extraordinary light. Because of that, we have to make sure that the incident light's polarization direction is the same as the LC extraordinary light direction (optical axis direction), which is the rubbing direction for the homogeneous alignment configuration.

To obtain multiple angles, we stack several layers of this LC–PMMA composite blazed grating with different grating periods as shown in Fig. 2. During the stacking, the top grating's period is made to be twice the period of the bottom grating to make all steering angles clearly resolvable. By applying different driving conditions on each layer, we can easily achieve multiple steering angles. The available number of steering angles is 2^N, where N is the number of stacked layers; i.e., in Fig. 2 the output can be one of four different outputs depending on the driving condition combinations. In Section 3 we describe the experimental demonstration of 16 dynamically addressable angles by stacking four layers with a small cross talk.

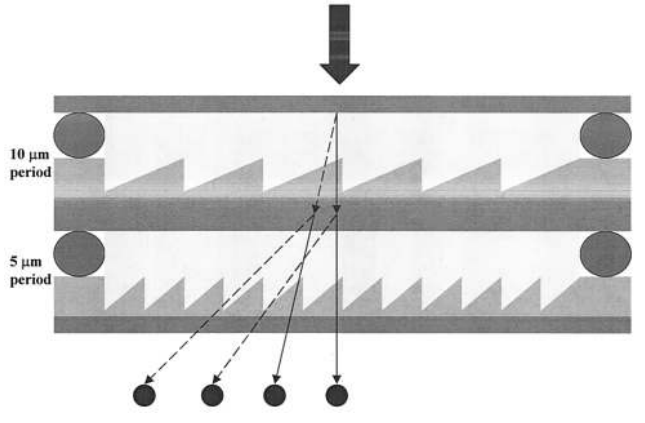

Fig. 2. Multiple-layer stacking concept to achieve multiple deflector angles.

3. Design Considerations

A. Liquid-Crystal Physics

When the driving voltage is applied, the LC molecule director tends to align itself along the electric field direction. According to the Frank elastic continuum theory,[20] the LC molecule director distribution will be stable when its net free energy is minimized. The net free energy F_{net} of the LC molecule director is given by

$$F_{\text{net}} = \frac{1}{2}\int_0^{\infty} \{K_{11}(\nabla \cdot \mathbf{n})^2 + K_{22}[\mathbf{n} \cdot (\nabla \times \mathbf{n})]^2 + K_{33}[\mathbf{n} \times (\nabla \times \mathbf{n})]^2 - \mathbf{D} \cdot \mathbf{E}\}\mathrm{d}V, \quad (1)$$

where K_{11} is the splay constant, K_{22} is the twist constant, and K_{33} is the bend constant. These constants correspond to S deformation, T deformation, and B deformation. $\mathbf{D}$ is the electric displacement, and $\mathbf{E}$ is the electric field. The molecule director is $\mathbf{n}(x, y, z)$. During the numerical modeling of the LC electro-optics effect, we made three assumptions: (1) strong anchoring at both surfaces, which means that the boundary condition is defined exclusively by the surface orientation angle; (2) no twist orientation is involved, which makes the K_{22} term in Eq. (1) disappear; and (3) one-dimensional modeling only, which implies $E_x = E_y = 0$. On the basis of these three assumptions, the simplified formula from Eq. (1) can then be written as

$$F_{\text{net}} = \frac{1}{2}\int_0^{L} (K_{11}\cos^2\theta + K_{33}\sin^2\theta)\left(\frac{\mathrm{d}\theta}{\mathrm{d}z}\right)^2 \mathrm{d}z - \frac{1}{2\epsilon_0}\int_0^{L} \frac{{D_z}^2}{\epsilon_{\perp}\cos^2\theta + \epsilon_{\parallel}\sin^2\theta}\,\mathrm{d}z, \quad (2)$$

where ϵ_0 is the dielectric constant in free space; D_z is the electric displacement along the Z direction; and $\epsilon_{\perp}$ and $\epsilon_{\parallel}$ are the dielectric constants of perpendicular and parallel direction to the electrical field, respectively. By using the variational calculus method,[21] we can change this integral equation into a differen-

tial equation that is obtained as follows (see Appendix A):

$$\left(\frac{\mathrm{d}z}{\mathrm{d}\theta}\right)^2 = \frac{K_{11}(1 + K \sin^2 \theta)}{C - \dfrac{D_z^{\,2}}{\epsilon_0 \epsilon_\perp (1 + r \sin^2 \theta)}}. \tag{3}$$

In Eq. (3), $K = (K_{33} - K_{11})/K_{11}$, $r = (\epsilon_\parallel - \epsilon_\perp)/\epsilon_\perp$, $C = D_z^{\,2}/[\epsilon_0 \epsilon_\perp (1 + r \sin^2 \theta_m)]$, and θ_m is the largest orientation angle that is located in the middle of the whole thickness. Numerically solving Eq. (3) with the orientation angles at the two boundary layers, we obtain the molecule director distribution inside the whole cell at a given driving voltage.

We need to perform one more step to obtain the LC's refractive-index information. From Section 2 we know that LC is an anisotropic birefringent material. Using the well-known formula for an anisotropic medium's index ellipse, we obtain the distribution of refractive index for extraordinary light inside the LC cell:

$$n_e(\theta_z) = \frac{n_o n_e}{(n_o^{\,2} \cos^2 \theta_z + n_e^{\,2} \sin^2 \theta_z)^{1/2}}, \tag{4}$$

where θ_z is the orientation angle and n_e and n_o are the LC's extraordinary and ordinary refractive index, respectively. It is more convenient, from a practical point of view, to use the effective refractive index of the whole cell for further discussion. It is given by

$$n_{\mathrm{eff}} = \frac{1}{L} \int_0^L n_e(z) \mathrm{d}z. \tag{5}$$

We determine the phase delay between ordinary and extraordinary light after passing through the medium as follows:

$$\delta = \frac{2\pi}{\lambda} \int_0^L [n_e(z) - n_o] \mathrm{d}z. \tag{6}$$

The homogeneous aligned nematic configuration[20] is chosen for our deflector because this configuration features a index modulation larger than those of the other configurations. This lowers our blazed-grating depth requirement for reaching the 2π phase delay that corresponds to the first diffraction order. This smaller depth requirement also offers us a quicker switching time. In the homogeneous configuration, we produce a strong parallel alignment along the surface of both layers by spin coating an anchoring chemical agent and then rubbing the surface. The elasticity of the LC, the applied electrical field, and the surface anchoring chemicals result in a symmetrical smooth rotation of the molecule director inside the nematic film. Figure 3 illustrates the homogeneous alignment configuration's molecule director distribution along the cell depth direction when a field is applied. The chosen LC material is Merck E7, whose refractive indices at a 633-nm wavelength for extraordinary and ordinary light are 1.737 and

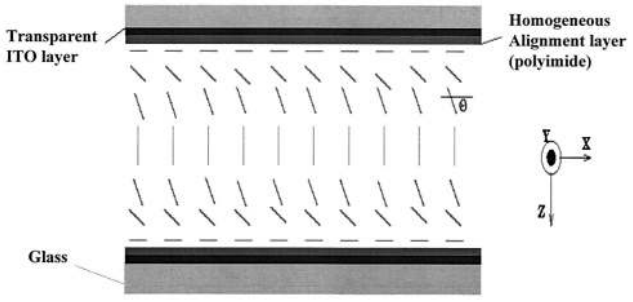

Fig. 3. Homogeneous alignment configuration.

1.5185, respectively.[22] E7 is a eutectic mixture of a number of cyanobiphenyls and cyanoterphenyls with a positive dielectric anisotropy, $\epsilon_\parallel \approx 18$ and $\epsilon_\perp \approx 6$, at a 1-kHz frequency and at room temperature.[23] Figure 4 shows the calculation results for an orientation-angle distribution with different driving voltages. As can be seen, the director orientation angle is increased with the magnitude of the driving voltage. The middle layer of the cell has the largest orientation angle for each driving voltage, reaching 90° when the voltage is large. After determining the orientation-angle distribution inside the cell at different voltages, we can easily calculate the effective refractive index (for extraordinary light) with the driving voltage. Figure 5 shows that the refractive index decreases continuously as the driving voltage increases. Ideally it can be swept from n_e to n_o when the driving voltage is varied from 0 to a very large value (assuming that a nonlinear effect does not occur). This electrically controlled birefringence is approximately 0.2 for E7 within 5 V. There is an interesting feature in Fig. 5. The variation of the refractive index happens only after a certain value, i.e., approximately 0.9 V for the E7 material. This is the so-called threshold voltage for the LC material with the homogeneous alignment configuration. The value of this threshold voltage is only a function of the material physical parameters, such as viscosity constant and elastic constant, and it is not changed

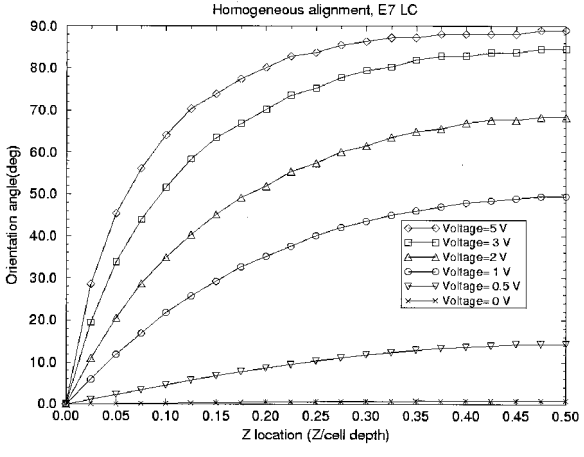

Fig. 4. Modeling results for homogeneous alignment orientation-angle distribution.

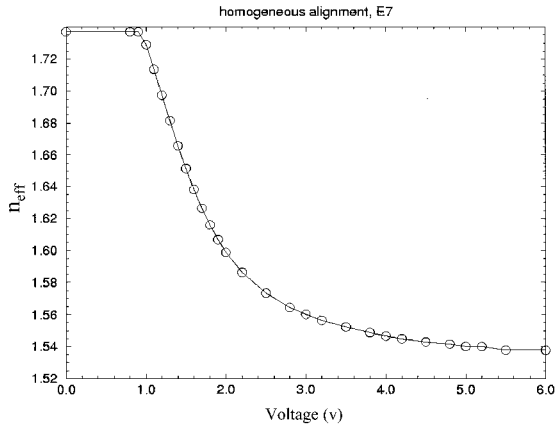

Fig. 5. Modeling results for homogeneous alignment refractive index.

with the cell's thickness. We will use this numerical tool for predicting the refractive index of the LC layer in the subsequent design of the deflector.

B. Diffraction Analysis

To understand the behavior of this device, a detailed analysis of the blazed-grating diffraction is also necessary. Considering that the device has a fairly large feature size relative to the illumination wavelength, we use scalar diffraction theory for its simplicity and fast modeling time.

As illustrated in Fig. 6, the whole aperture transmittance $T(x)$ of the blazed grating is considered as a prism function $P(x)$ convolved with a periodic grating function $G(x)$:

$$T(x) = P(x) * G(x). \tag{7}$$

The periodic grating function is

$$G(x) = \sum_{m=1}^{N} \delta(x - mp)\mathrm{rect}\left(\frac{x}{A}\right), \tag{8}$$

where p is the blazed grating period and A is the illumination width. For the prism function $P(x)$, the fabrication error shown in Fig. 6 is also taken into account in this analysis as follows:

$$P(x) = \mathrm{rect}\left(\frac{x}{p}\right)\exp[i\Delta(x)], \tag{9}$$

where $\Delta(x)$ is defined as

$$\Delta(x) = \frac{2\pi}{\lambda}(n_1 - n_2)x\tan\theta \qquad (0 < x \le a),$$

$$\Delta(x) = \frac{2\pi}{\lambda}(n_1 - n_2)\mathrm{d} \qquad (a < x < p), \tag{10}$$

where the duty cycle is defined as a/p. Then the far field is the Fourier transform (FT) of this aperture transmittance:

$$E(x) = \mathrm{FT}[T(x)] = \mathrm{FT}[P(x)] \cdot \mathrm{FT}[G(x)] = P \cdot G, \tag{11}$$

where P results in a $\mathrm{sinc}(x) = \sin(\pi x)/\pi x$ function profile in the far field, and its peak location is defined by the prism depth d. G defines the diffraction-order locations and samples the prism-produced sinc function to define the final diffraction pattern. If the blazed grating is well designed so that the prism-produced $\mathrm{sinc}(x)$ function profile peaks at the first diffraction-order position, then theoretically the first order will have 100% diffraction efficiency and all other diffraction orders will have zero diffraction efficiency. This also suggests that, even for one layer of LC–PMMA grating, it is possible to obtain multiple deflection angles if the PMMA blazed-grating depth is large enough so that the phase difference between PMMA and LC could reach the multiple integer numbers of 2π, say, 4π or 6π, which correspond to second or third diffraction order blazed, respectively. However, for those cases, the switching speeds would be slow because of the LC's large thickness, since the response time of the LC device is proportional to the square of its thickness; i.e., a second-order blazed deflector's switching speed is four times slower than that of a first-order blazed deflector.

For our LC–PMMA blazed grating, the illumination wavelength is 633 nm, the refractive index of PMMA is taken as 1.49 (roughly the ordinary index of the LC), and the refractive index of extraordinary light for LC E7 is taken as 1.737. With the ideal profile (100% duty cycle), the blazed grating's optimal depth is calculated to be 2.67 μm as shown in Fig. 7.

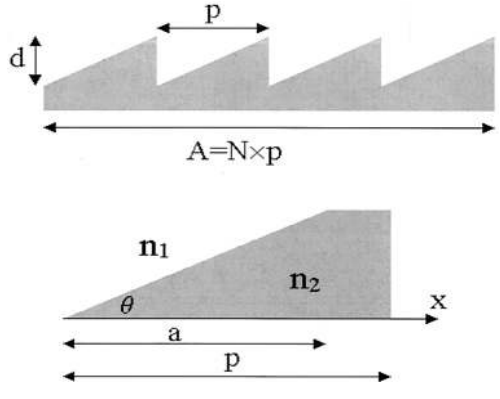

Fig. 6. LC blazed-grating diffraction model.

C. Driving Voltage Loss and Nonuniformity

For our device, the driving voltage is applied between two ITO layers. However, the PMMA blazed grating is made on top of the substrate's ITO layer to simplify the fabrication process. This reduces the driving voltage on the LC because PMMA is a poor conductor. (The conductivity is reported to be approximately 10^{-11} S/m in the glassy state at room temperature with a dielectric constant of approximately 3.[23]) Also, the PMMA blazed-grating profile results in different driving voltages on the LC at different locations. Figure 8 illustrates the above-

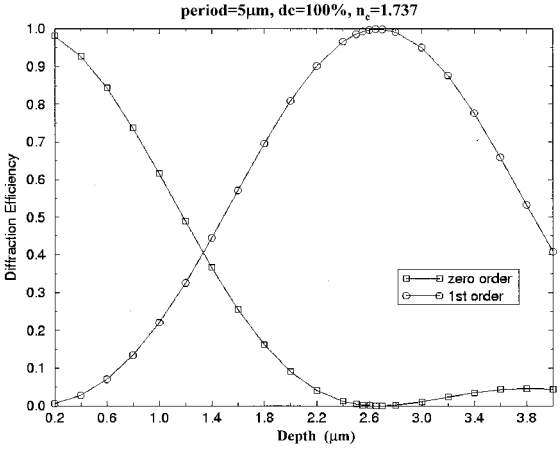

Fig. 7. Optimization of the blazed-grating depth. dc, duty cycle.

mentioned driving voltage loss and voltage nonuniformity issues.

The driving voltage loss calculation can be determined from Maxwell's equations boundary condition on the electric field:

$$\mathbf{D}_{\mathrm{LC}_n} - \mathbf{D}_{\mathrm{PMMA}_n} = \sigma = 0, \tag{12}$$

where $\mathbf{D}$ is the electric displacement and σ is the surface charge density, which is zero in our analysis. On the basis of the dielectic constants of the E7 LC and the PMMA, and considering that there is a residual PMMA layer at the bottom of the LC–PMMA grating, we can obtain the effective voltage V_{eff} on the LC–PMMA grating from the following equation:

$$V_{\mathrm{eff}} = \frac{1 - r}{1 + \beta r} V_{\mathrm{apply}}, \tag{13}$$

where V_{apply} is the applied voltage on the two ITO layers and r is the ratio of the residual PMMA layer thickness and the depth summation of spacer and PMMA grating. β is a dielectric-related constant, which here turns out to be approximately 5. From

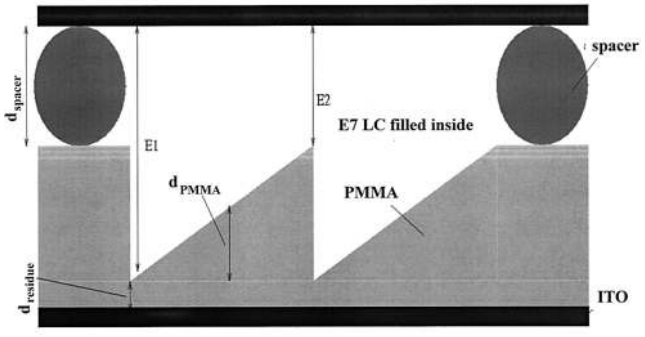

Fig. 8. LC blazed-grating deflector's driving voltage loss and nonuniformity. E1 and E2 represent the electrical field in the electrical domain.

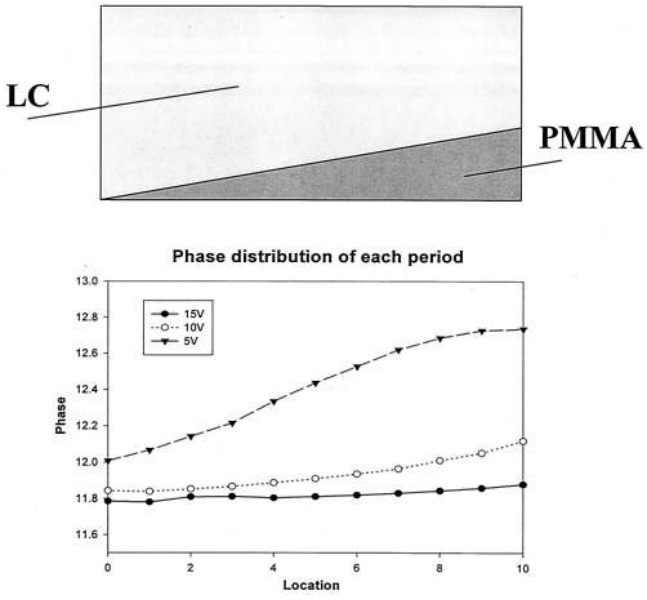

Fig. 9. LC blazed-grating deflector index matching.

this we can define the actual driving voltage on the V_{LC} at different positions:

$$V_{\mathrm{LC}}(x) = \frac{1 - rr(x)}{1 + \beta rr(x)} V_{\mathrm{eff}}, \tag{14}$$

where $rr(x)$ is the depth ratio between the PMMA grating and the spacer at different locations. From our calculations, only 18–60% of the driving voltage is actually applied on the LC with the parameters of a 5-μm spacer, a 0.6-mm residual uniform PMMA layer, and a PMMA grating depth of 2.67 μm assuming a 100% duty cycle.

The phase delay caused by the LC–PMMA composite structure at different locations within one period was calculated at different applied voltages. Figure 9 shows that, although the voltage on the LC is different at different positions, the phase delays at those positions become more uniform at higher voltage. The reason is that, at locations with thinner PMMA, the driving voltage loss is less, which results in a smaller LC refractive index. At locations with thicker PMMA, the voltage loss is greater so that the refractive index of the LC remains relatively large, which compensates for the low index of PMMA to reach roughly the same phase delay as the thinner PMMA parts. Normally it is difficult to reach index matching between the LC and PMMA at every location because of the applied voltage's nonuniform distribution. However, we can reach a uniform phase distribution at every location at a higher voltage, which ensures the device's successful operation. In this sense, it is more meaningful to discuss the phase matching rather than the index matching.

4. Fabrication Process

The PMMA blazed gratings were fabricated by direct-write e-beam lithography.[19,24] We prepared the

ITO-coated substrates by spinning in succession five layers of PMMA to achieve a total thickness of 3.3 μm. Each deposition sequence included a bakeout for 60 min at 170 °C. Prior to exposure, the sample was overcoated with 10 nm of aluminum, which acted as a discharge layer preventing defocusing that is due to surface charge buildup. The e-beam exposure patterns for the blazed grating were composed of square pixels (0.5 μm for 5-μm period grating, 1 μm for 10-μm period grating, etc.). Within each pixel, the e-beam spot was rastered to expose the pixel area uniformly. We determined the pixel doses from the desired depths, taking into account the nonlinear depth versus the dose response of the PMMA and the e-beam proximity effect (backscattered dose from the substrate). The proximity effect for these substrates (50-kV acceleration voltage) was measured to have a Gaussian $1/e$ radius of 10.75 μm and an integrated strength of 0.5 of the initial dose. Fourier-transform deconvolution of the proximity effect function was performed on the pixelized dose profile as described in Refs. 19 and 24.

We exposed the gratings using a JEOL Model JBX-5DII e-beam lithography system at 50 kV with a beam current of 4 nA, which corresponds to a spot size of 0.3 μm. This is larger than would be used for precision lithography, but it somewhat smoothes the surface of the blazed grating and reduces the writing time. The total exposure time for each grating with an area 3.2 mm × 3.2 mm was 70 min. After exposure, the aluminum overcoat was removed and the grating was developed in pure acetone by use of a Solitec spinner equipped with an electronically controlled Tridak resist dispenser. The substrate was spun at 1000 rpm while the acetone was squirted down at the center of rotation. At the end of 8 s, the acetone was abruptly cut off and replaced by a blast of dry nitrogen. This quenched the development and at the same time dried the surface of the PMMA. Additional development steps with times as short as 0.5 s were used to achieve the desired grating depth. We gauged the depth by measuring the diffraction from a computer-generated hologram (on the same substrate) that was designed to produce a null zero order. Near the final depth, the grating profile was measured directly with a Digital Instruments Nanoscope III atomic force microscope (AFM).

We fabricated four PMMA samples with grating periods of 5, 10, 20, and 40 μm. Figure 10 shows the final surface profile of the 10-μm period grating. As can be seen, the blazed slope is quite good although the top plane has a small portion of flatness, which induced a non-100% duty cycle. We calculated this nonideal duty cycle's effect on the diffraction efficiency using the above-discussed model; Fig. 11 shows the calculation result. It clearly shows that the nonoptimal duty cycle degrades the performance significantly. Also, a 50% duty cycle blazed grating has zero diffraction efficiency into the first diffraction order, which also validates our numerical modeling's correctness to some degree. Nevertheless, the 40-μm sample's duty cycle is much better than that of the 10-μm sample. More contour surface parameter verifications are discussed in Section 5.

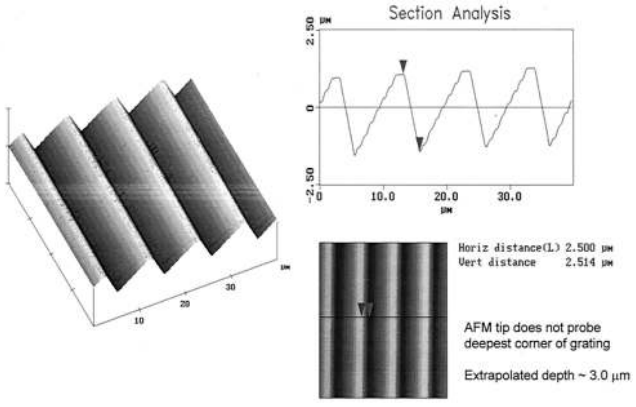

Fig. 10. Surface profile of a 10-μm period grating measured by an AFM.

Our fabrication process (shown in Fig. 12) is as follows. First, a glass plate is coated with a 20-Ω/sq ITO transparent electrode to form the ITO glass. A polyimide solution [1% mass in n-methyl-2-pyrrolidone (NMP); here NMP is used for the polyimide thinner] is spun onto the ITO glass at 3000 rpm for 40 s and then baked at 200 °C for 30 min. This polyimide-coated ITO glass is then rubbed unidirectionally on a cloth to form a uniaxially buffered alignment layer. The pretreated ITO cover glass is put on top of the PMMA blazed grating at a microscopic distance set by small drops of a mixture of chopped glass fibers and Norland91 UV-cured optical adhesive 91, which are deposited on the periphery of the active area of the cell. The resulting cavity is then filled with Merck E7 at room temperature, since the PMMA cannot sustain high temperature because of its ~110 °C melting point. The completed one layer of this device is approximately 2.5-mm thick with an approximately 1.2-mm-thick glass substrate. Note that our PMMA grating sample is not rubbed. The reason is that the e-beam-fabricated blazed-grating

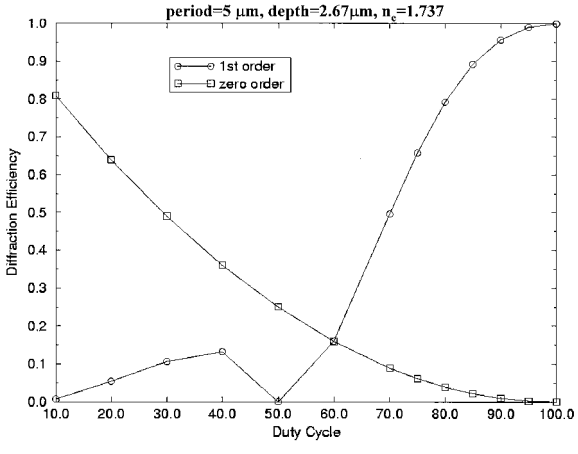

Fig. 11. Influence of blazed-grating duty cycle on diffraction efficiency.

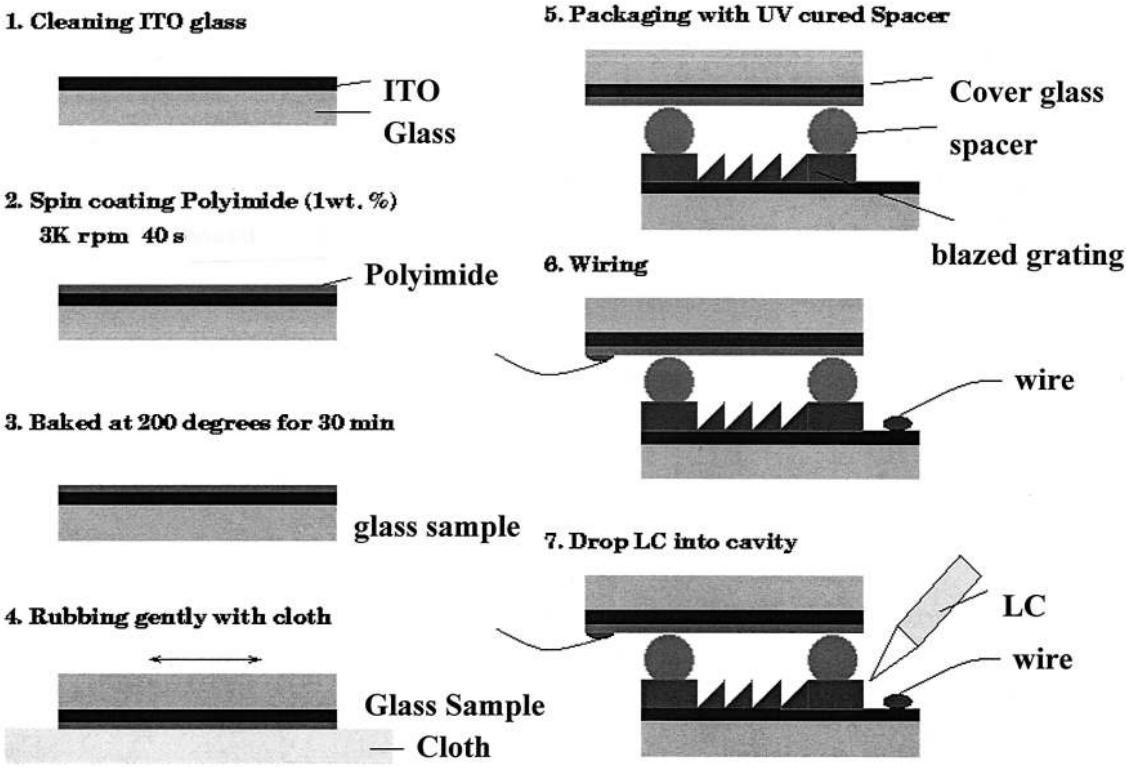

Fig. 12. LC blazed-grating deflector packaging process.

surface has tiny grooves along the blazed slope (see Fig. 10) that can be utilized as the natural alignment layer if we fill the LC along the groove direction. However, it is important that the cover plate's alignment direction be parallel to the grating groove direction to reach the homogeneous alignment configuration.

The following are some considerations for stacking multiple layers of this LC–PMMA composite grating. First, to make full use of each layer's manufacturing-limited effective area, an accurate alignment of those samples is necessary. This can be achieved by continuous adjustment monitored by a microscope. Second, the extraordinary axis directions of each layer must be aligned during stacking because the device is operated in a polarization mode. Third, each layer's deflection direction should be the same so that each layer's deflection can be monotonically accumulated. Finally, to reduce scattering, the best stacking order for illumination is 40, 20, 10, and 5 μm. Illumination of the 40-μm grating layer first will generate the smallest deflection angle (approximately 0.9°), so that for subsequent layers the incident angle can still be considered as approximately normal.

5. Experiment and Discussion

The experimental setup is shown in Fig. 13. A polarized beam is incident on the deflector with its polarization direction parallel to the LC alignment direction because it is a polarized beam deflector. Four individually controllable dc-balanced 1-kHz square waveforms are applied onto four stacked LC blazed gratings. A detector mounted on a scanning translation stage measures the far-field intensity at each diffraction order to calculate the diffraction efficiency.

A. Determination of Sample Profile Parameters

Before stacking the LC–PMMA layers, we need to determine the PMMA blazed-grating profile parameters accurately by combining three measurements. The first step is to use the AFM profile measurement data as shown in Fig. 10. However, because of the finite size of the AFM tip and the sharp transition corners of the blazed grating, the AFM tip does not typically probe the deepest region of the grating surface, so the depth measurement is not quite reliable. Nevertheless, it does at least accurately give us the duty cycle information, which is used for the next two

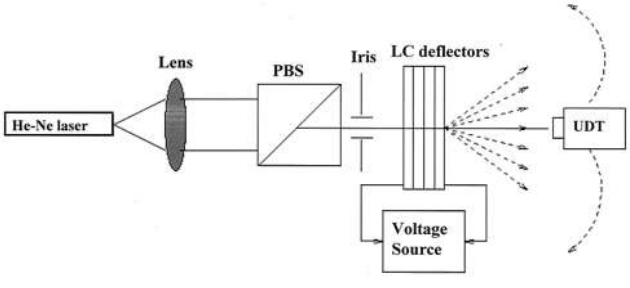

Fig. 13. Characterization of the experimental setup. PBS, polarization beam splitter.

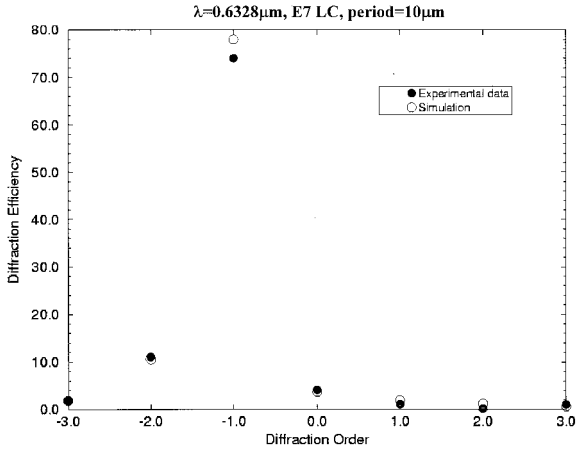

Fig. 14. Determination of grating surface profile parameters.

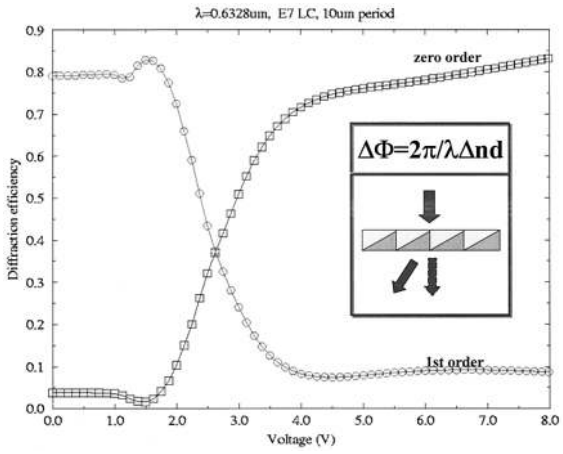

Fig. 15. LC blazed-grating diffraction efficiency versus driving voltage.

steps. The second step is to compare the experimental measurement with the theoretical prediction of the diffraction from the PMMA blazed grating in free space (no LC). The third step is implemented after the PMMA blazed grating is filled with LC. This is to compare the experimental measurement and theoretical prediction of the diffraction from the LC–PMMA composite grating without any applied voltage. Figure 14 shows an example of the diffraction measurement we made and the optimal modeled contour for the 10-μm sample. The optimal parameters, given by the best match between experimental data and the model prediction of the diffraction orders, are a 2.74-μm depth and 82% duty cycle for the sample. Similarly, the other sample profile parameters are finalized as follows: the 5-μm sample is 2.85 μm deep with 90% duty cycle, the 10-μm sample is 2.74 μm deep with 82% duty cycle, the 20-μm sample is 2.71 μm deep with 94% duty cycle, and the 40-μm sample is 2.87 μm deep with 99% duty cycle.

B. Characterization of Single-Layer Deflector

During this characterization, we measured the zero and first diffraction order's diffraction efficiency while scanning the driving voltage from 0 to 8 V for each LC blazed grating. The experimental data for the 10-μm sample are plotted in Fig. 15. Note that the diffraction efficiency at a small voltage (1.5 V) is actually higher than that at zero voltage for the OFF state. The reason is that, as suggested from the profile parameters definition, the fabricated PMMA sample depth is slightly higher than the optimal design depth. As discussed above in the scalar diffraction analysis, the microprism produces a $\mathrm{sinc}(x)$ function that could shift the blaze location to different diffraction orders, corresponding to different prism depths reaching a 2π phase delay. The phase delay difference $\Delta\phi$ between LC and PMMA is

$$\Delta\phi = \frac{2\pi}{\lambda}\Delta n d, \tag{15}$$

where Δn is the refractive-index difference between PMMA and LC and λ is the illumination wavelength. If the depth d is slightly larger than the optimal depth, $\Delta\phi$ is larger than expected so that the peak will be shifted slightly to the right side of the desired position. We can shift this $\mathrm{sinc}(x)$ function peak back to the desired location by reducing Δn and hence reaching the optimal $\Delta\phi$. This technique is based on the fact that LC's refractive index can be modulated when a driving voltage is applied. We call this small voltage the virtual OFF voltage of the LC deflector.

Using this virtual OFF voltage method, we first tested the four LC deflectors separately. The maximum applied voltage was 15 V; considering the voltage loss calculated before, the real voltage driving the LC is approximately 2.7–9 V. All measurement

Table 1. Diffraction Gratings of the Four LC–PMMA Blazed Gratings (%)

	Period (μm)							
	5		10		20		40	
Order	ON	OFF	ON	OFF	ON	OFF	ON	OFF
2	1.4	2.48	0.71	0.85	0.37	0.29	0.73	0.31
1	2.3	2.15	2.47	0.53	1.11	0.44	2.41	0.95
0	87.65	2.56	88.62	2.03	93.62	1.86	88.99	7.71
−1	2.4	81.68	2.64	82.90	1.56	87.50	4.83	83.42
−2	1.34	2.05	0.57	0.84	0.45	5.34	1.22	5.24

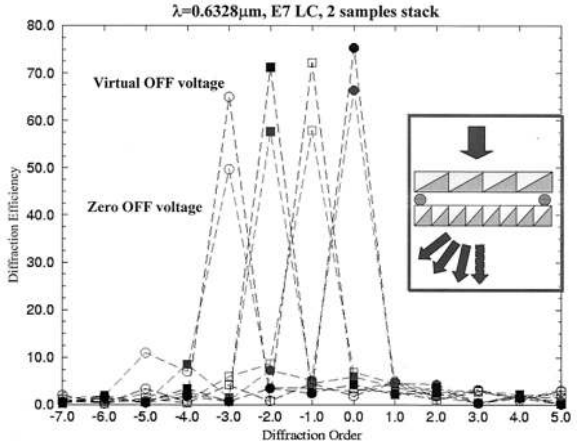

Fig. 16. Comparison between the real OFF state and the virtual OFF state.

data are listed in Table 1. The measured diffraction efficiencies at the ON and OFF states are all in the range of 81.7–93.6%. The cross talk turns out to be very small. (The intensity ratios between the brightest spot and the second brightest spot are in the range of 32–60.)

Finally, we measured the response time of this blazed-grating deflector by observing the first diffraction-order intensity variation during the switching transient period after 15-V applied voltage was turned on. The measured rise and fall times were approximately 8 and 15 ms, respectively.

C. Characterization of Multiple-Layer Deflector

After characterizing the single-layer deflector performance, we stacked the samples to demonstrate 4, 8, and finally 16 steering angles. Again, the virtual OFF voltage method was applied. Figure 16 shows the big performance improvement achieved by this virtual OFF voltage method. The diffraction efficiency with the virtual OFF voltage applied is at least 10% higher than that without applying voltage. Correspondingly, the contrast ratio is dramatically enhanced. The steering efficiencies of the four angles ranged from 67 to 75%. The contrast ratio between the strongest and second strongest spots is in the range of 15–21.

Table 2. Measurement Data of the Four Stacked-Grating 16-Angle Deflector

5 μm	10 μm	20 μm	40 μm	Angle	Diffraction Efficiency	Contrast Ratio 1st/2nd
1	1	1	1	0.0	0.5759	17.7
1	1	1	0	0.9	0.5661	17.5
1	1	0	1	1.8	0.5637	13.5
1	1	0	0	2.7	0.4400	10.2
1	0	1	1	3.6	0.5308	14.7
1	0	1	0	4.5	0.4024	12.6
1	0	0	1	5.4	0.5225	10.4
1	0	0	0	6.3	0.4125	11.9
0	1	1	1	7.2	0.4336	14.4
0	1	1	0	8.1	0.3627	12.7
0	1	0	1	9.0	0.4833	10.9
0	1	0	0	9.9	0.3734	9.8
0	0	1	1	10.8	0.4402	13.5
0	0	1	0	11.7	0.3410	9.9
0	0	0	1	12.6	0.4023	9.4
0	0	0	0	13.5	0.2892	9.1

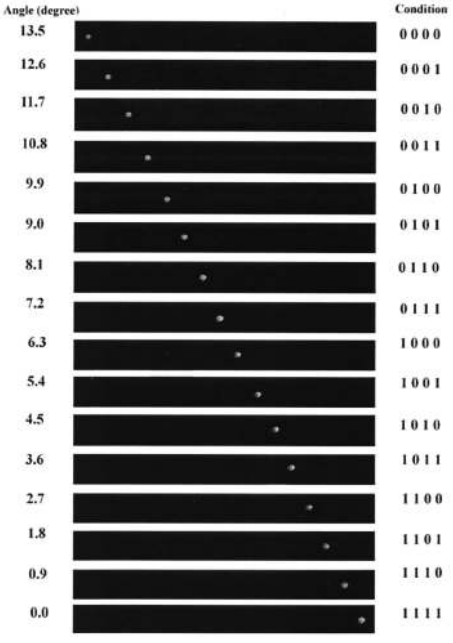

Fig. 17. Photographs of the 16-angle deflector diffracted spots.

Finally, the measurement data for the 16 steering-angle stacked deflector are tabulated in Table 2. Experimentally demonstrated steering efficiency ranges from 28.9 to 57.6%, and the contrast ratio ranges from 9.1 to 17.7. Figure 17 shows pictures of the laser beam steering spots as well as the driving condition. The 16 steering angles (0°–13.5°) are obtained with a resolution of 0.9°. The fluctuation of the diffraction efficiency is contributed by the nonperfect blazed-grating samples and the scattering between LC and different layers of gratings, which reduce the bending powers of the composite grating layers.

6. Summary and Discussion

A multiple-angle LC blazed-grating beam deflector has been developed. Sixteen steering angles with a contrast ratio as high as 18 have been demonstrated. A detailed analysis of the LC–PMMA blazed-grating deflector was carried out to aid in the deflector's design. A manufacturing offset compensation technique was proposed and demonstrated to greatly enhance the deflector's performance.

In optical networking and optical asynchronous transfer mode switching, as well as optical holographic applications, a beam deflector with the capability of addressing a large number of steering angles is desirable. For example, several hundreds of angles are commonly needed for a typical holographic data storage system. One straightforward approach

to accomplish this is to stack more layers of the LC–PMMA composite because the available addressing angles are 2 to the power of the number of layers. To increase the number of layers beyond the four demonstrated in this paper, each individual layer's performance must be further optimized. One can accomplish this by fine tuning the PMMA blazed-grating fabrication process to achieve a better blazed profile and depth control, depositing antireflection coatings on each layer to reduce the scattering inside the stacked layers, and using LC materials that offer better index matching with PMMA. However, this adds a challenge to the device's fabrication process, and hence the cost is a concern. Furthermore, the device's optical throughput will be greatly decreased when more layers are stacked together.

A more promising approach is to build a hybrid device by use of an electrically generated blazed grating combined with the previously described cascading approach.[7,25] Patterned electrodes and an uniform ITO layer coated on the cover glass electrically drive a LC layer to build up a virtual blazed grating inside the LC medium. The virtual blazed-grating's period can be programmed when appropriate voltages are assigned along these electrodes. This generates a multiple-angle addressing device. We can make this electrically generated blazed grating only with a relatively large period, which yields a small deflection angle. Therefore it is used as a fine scanning component. The LC–PMMA blazed-grating period, on the other hand, is normally small and therefore it is used as the coarse scanning component. By attaching these coarse and fine scanning components, one can achieve a steering device with a large number of addressable angles. For example, assume we combine the demonstrated four layers of LC–PMMA blazed grating with the electrically generated blazed grating whose period can be programmed to be 80, 160, 320, 640, and 1280 μm. The number of addressable angles becomes $16 \times 2^5 = 512$. When compared with the simple cascading approach, in which nine layers of LC–PMMMA grating is needed to obtain 512 angles, this proposed hybrid approach is clearly better.

As a final note on this device, the device's switching speed is in the millisecond range because of the nematic LC's physical limitation. It is well known that ferroelectric liquid crystal features a much faster switching speed. One possible solution is to choose ferroelectric LC rather than nematic LC as the working medium. When we consider that the device is basically a binary switch on each layer, the ferroelectric LC's binary operation mechanism is not a problem. The only overhead would come from the complicated ferroelectric LC driver accessory and finding a suitable material with index matching to PMMA.

Appendix A: Major Derivation Steps from Equation (2) to Equation (3)

According to the variation calculus method, a typical minimization problem of the type $\int_0^L F[z, \theta(z), \mathrm{d}\theta(z)/\mathrm{d}z]\mathrm{d}z$ can be converted into the corresponding Euler equation

$$F_\theta - \frac{\mathrm{d}\left(F_{\frac{\mathrm{d}\theta}{\mathrm{d}z}}\right)}{\mathrm{d}z} = 0.$$

So the Euler equation for Eq. (2) can be converted into

$$(K_{11}\cos^2\theta + K_{33}\sin^2\theta)\frac{\mathrm{d}^2\theta}{\mathrm{d}z^2} + (K_{33} - K_{11})\sin\theta\cos\theta\left(\frac{\mathrm{d}\theta}{\mathrm{d}z}\right)^2 = \frac{D_z^{\,2}}{\epsilon_0}\frac{(\epsilon_\parallel - \epsilon_\perp)\sin\theta\cos\theta}{(\epsilon_\perp\cos^2\theta + \epsilon_\parallel\sin^2\theta)^2}. \quad \text{(A1)}$$

When Eq. (A1) is multiplied by $2\mathrm{d}\theta/\mathrm{d}z$, note that the right-hand side of Eq. (A1) equals

$$-\frac{1}{2}\frac{\mathrm{d}\left(\frac{1}{\epsilon_\perp\cos^2\theta + \epsilon_\parallel\sin^2\theta}\right)}{\mathrm{d}\theta},$$

as well as

$$\frac{1}{2}\frac{\mathrm{d}(K_{11}\cos^2\theta + K_{33}\sin^2\theta)}{\mathrm{d}\theta} = (K_{33} - K_{11})\sin\theta\cos\theta,$$

we than have

$$\frac{\mathrm{d}\left[(K_{11}\cos^2\theta + K_{33}\sin^2\theta)\left(\frac{\mathrm{d}\theta}{\mathrm{d}z}\right)^2\right]}{\mathrm{d}z} = -\frac{D_z^{\,2}}{\epsilon_0}\frac{\mathrm{d}\left(\frac{1}{\epsilon_\perp\cos^2\theta + \epsilon_\parallel\sin^2\theta}\right)}{\mathrm{d}z}, \quad \text{(A2)}$$

resulting in Eq. (3).

This research was supported by the U.S. Air Force Rome Laboratory and the National Science Foundation Engineering Research Center for Neuromorphic Systems Engineering at the California Institute of Technology. X. Wang and D. Psaltis thank Jean-Jacques Drolet for his valuable contribution at the early stage of this research.

References

1. K. Hirabayashi, T. Yamamoto, and M. Yamaguchi, "Free-space optical interconnections using liquid crystal microprism arrays," Inst. Phys. Conf. Ser. **139,** 195–198 (1994).
2. K. Hirabayashi and T. Kurokawa, "Liquid crystal devices for optical communication and information processing systems," Liq. Cryst. **14,** 307–317 (1993).
3. D. Faklis and G. M. Morris, "Diffractive optics technology for display applications," in *Projection Displays*, M. H. Wu, ed., Proc. SPIE **2407,** 57–61 (1995).
4. J. J. Drolet, E. Chuang, G. Barbastathis, and D. Psaltis, "Compact, integrated dynamic holographic memory with refreshed holograms," Opt. Lett. **22,** 552–554 (1997).

5. Q. Chen, Y. Chiu, and D. D. Stancil, "Guide-wave electro-optic beam deflector using domain reversal in $LiTaO_3$," J. Lightwave Technol. **12,** 1401–1404 (1994).
6. J. A. Thomas, M. Lasher, Y. Fainman, and P. Soltan, "PLZT-based dynamic diffractive optical element for high-speed, random-access beam steering," in *Optical Scanning Systems: Design and Applications*, L. Beiser and S. F. Sagan, eds., Proc. SPIE **3131,** 124–132 (1997).
7. D. P. Resler, D. S. Hobbs, R. C. Sharp, L. J. Friedman, and T. A. Dorschner, "High-efficiency liquid-crystal optical phased-array beam steering," Opt. Lett. **21,** 689–691 (1996).
8. E. Schulze and W. Reden, "Diffractive liquid crystal spatial light modulators with fine-pitch phase gratings," in *Liquid Crystal Materials, Devices, and Displays*, R. Shashidhar and U. Efron, eds., Proc. SPIE **2408,** 113–120 (1995).
9. G. Williams, N. J. Powell, A. Purvis, and M. G. Clark, "Electrically controllable liquid crystal Fresnel lens," in *Current Developments in Optical Engineering and Commercial Optics*, R. E. Fischer, H. M. Pollicove, and W. J. Smith, eds., Proc. SPIE **1168,** 352–357 (1989).
10. L. H. Domash, T. Chen, B. N. Gomatam, C. M. Gozewski, R. L. Sutherland, L. V. Natarajan, V. P. Tondiglia, T. J. Bunning, and W. W. Adams, "Switchable-focus lens in holographic polymer-dispersed liquid crystal," in *Diffractive and Holographic Optics Technology III*, I. Cindrich and S. H. Lee, eds., Proc. SPIE **2689,** 188–194 (1996).
11. R. L. Sutherland, "Electrically switchable volume holographic gratings in polymer-dispersed liquid crystals," Appl. Phys. Lett. **64,** 1074–1076 (1994).
12. J. Borel, J. C. Deutsch, G. Labrunie, and J. Robert, "Liquid crystal diffraction grating," U.S. patent 3,843,231 (20 October 1974).
13. A. F. Fray and D. Jones, "Large-angle beam deflector using liquid crystals," Electron. Lett. **15,** 358–359 (1975).
14. T. A. Dorschner and D. P. Resler, "Optical beam steering having subaperture addressing," U.S. Patent 5,093,747 (5 March 1992).
15. B. J. Cassarly, J. C. Ehlert, and D. J. Henry, "Low insertion loss high precision liquid crystal optical phased array," in *Free-Space Laser Communication Technologies III*, D. L. Begley and B. D. Seery, eds., Proc. SPIE **1417,** 110–121 (1991).
16. V. R. L. Sutherland and L. V. Natarajan, "Development of photopolymer liquid crystal composite materials for dynamic hologram applications," in *Diffractive and Holographic Optics Technology*, I. Cindrich and S. H. Lee, eds., Proc. SPIE **2152,** 303–313 (1994).
17. D. Armitage, "Silicon-chip liquid crystal display," in *Projection Displays*, M. H. Wu, ed., Proc. SPIE **2407,** 280–290 (1995).
18. T. Uchida, "Present and future trend of liquid crystal devices," in *Display Technologies*, S. Chen and T. Wang, eds., Proc. SPIE **1815,** 10–17 (1992).
19. P. D. Maker, D. W. Wilson, and R. E. Muller, "Fabrication and performance of optical interconnect analog phase holograms made by E-beam lithography," in *Optoelectronic Interconnects and Packaging*, R. T. Chen and P. G. Guilfoyle, eds., Vol. 62 of SPIE Critical Review Series (SPIE Press, Bellingham, Wash., 1996), pp. 415–430.
20. L. M. Blinov, "Electro-optical effects in liquid crystals," Sov. Phys. Usp. **17,** 658–672 (1975).
21. W. Press, B. Flannery, S. Teukolsky, and W. Vetterling, *Numerical Recipes in C*, 2nd ed. (Cambridge U. Press, New York, 1988).
22. Frank Allan, EM Industries, Inc., 7 Skyline Drive, Hawthorne, N.Y. (personal communication, 1996).
23. Z. Z. Zhong, D. E. Schuele, W. L. Gordon, K. J. Adamic, and R. B. Akins, "Dielectric properties of a PMMA/E7 polymer-dispersed liquid crystal," J. Polym. Sci. Polym. Phys. **30,** 1443–1449 (1992).
24. D. W. Wilson, P. D. Maker, and R. E. Muller, "Binary optics reflection grating for an imaging spectrometer," in *Diffractive and Holographic Optics Technology III*, I. Cindrich and S. H. Lee, eds., Proc. SPIE **2689,** 255–266 (1996).
25. X. Wang and D. Psaltis, "Liquid crystal on silicon beam deflector," in *Diffractive and Holographic Technologies, Systems, and Spatial Light Modulators VI*, I. Cindrich, S. H. Lee, and R. L. Sutherland, eds., Proc. SPIE **3633,** 160–169 (1999).